

# The reaction $\pi N \rightarrow \omega N$ revisited: the $\omega$ - $N$ scattering length

C. Hanhart, A. Sibirtsev, and J. Speth

<sup>a</sup>*Institut für Kernphysik, Forschungszentrum Jülich, D-52425 Jülich*

(Dated: November 14, 2018)

We reinvestigate the experimental data on  $\omega$ -meson production in pion-nucleon collisions [1, 2, 3] based on both an analytical approach and a Monte Carlo simulation. Our analysis allows us to study the kinematical peculiarities of the  $\pi^- p \rightarrow \omega n$  reaction at energies close to threshold. Based on the hypothesis, that the formalism derived in ref. [1] was applied improperly, the unusually strong energy dependence claimed for the near-threshold cross section is identified as a purely kinematical effect. Based on this hypothesis, we deduce an effective  $\pi^- p \rightarrow \omega n$  cross section that is larger by an order of magnitude compared to the one commonly used. In addition we extract a lower limit for the imaginary part  $\Im a_{\omega N}$  of the  $\omega N$  scattering length. We find a value of  $\Im a_{\omega N} = 0.24 \pm 0.05$  fm, which is significantly larger than that presently found in the literature.

PACS numbers: 11.55.Fv; 13.75.Jz; 13.85.Dz; 25.80.-e

Keywords: production of narrow resonances, properties of  $\omega$  mesons, medium effects

## I. INTRODUCTION

In Refs. [1, 2, 3] the reaction  $\pi^- p \rightarrow \omega n$  was measured at energies close to the nominal  $\omega$  production threshold. In Ref. [4] it was claimed that these experiments were interpreted incorrectly. In this work we reinvestigate the experiments using an event-by-event simulation as well as an analytical calculation. The purpose of this manuscript is two fold: Besides studying, if the reaction kinematics was treated properly in Refs. [1, 2, 3], we also take the opportunity to discuss in detail the method proposed in Ref. [1] for the near threshold production of narrow resonances, for it might prove usefull for upcoming experiments at modern accelerators.

The reaction  $\pi N \rightarrow \omega N$ , especially at energies close to the reaction threshold, attracts great interest for several reasons.

1) There is a large number of baryonic resonances that have been predicted theoretically but not yet observed experimentally [6]. Since almost all our knowledge about resonances is deduced from elastic  $\pi N$  scattering, to really resolve the issue of the missing resonances other channels must be studied. There are predictions of a number of baryonic resonances with masses from 1.8 to 2 GeV which might couple to the  $\omega N$  channel [7]. The  $\pi N \rightarrow \omega N$  data is an essential ingredient in any kind of analysis aimed at identifying baryonic resonances possibly coupled to the  $\omega$ -meson. A reliable extraction of the resonance properties implies the analysis of pion and photon induced data simultaneously for as many final states as possible [9, 10].

In the experiments described in Refs. [1, 2, 3] the squared matrix element  $|\mathcal{M}|^2$  was extracted from a measurement of the reaction  $\pi^- p \rightarrow \omega n$ . The authors claim to have measured a very strong near-threshold suppression, which might stem from the production of a baryonic

resonance in a  $p$ -wave. The measured differential cross sections, however, are isotropic. Up to now a suppression of the matrix element as reported in [1, 2, 3] cannot be understood theoretically [8]. In any case, the  $\pi^- p \rightarrow \omega n$  cross section is very important for resolving the existence of resonances not yet observed.

2) The  $\pi^- p \rightarrow \omega n$  data [3] are intensively used in the evaluation of the in-medium properties the of  $\omega$ -meson [11, 12, 13, 14]. The in-medium  $\omega$ -meson mass and width are commonly considered either for low finite  $\omega$  momenta  $p_\omega$  or at  $p_\omega=0$ . Within the  $t\rho$  approximation an additional in-medium collisional width  $\Delta\Gamma_\omega$  of the  $\omega$ -meson is given by the imaginary part of the forward  $\omega N$  scattering amplitude  $\Im f_\omega(0)$  as [15, 16, 17],

$$\Delta\Gamma_\omega = 4\pi \frac{m_N + m_\omega}{m_N m_\omega} \Im f_\omega(0) \rho_B, \quad (1)$$

where  $m_N$  and  $m_\omega$  are the free nucleon and  $\omega$ -meson masses, respectively, while  $\rho_B$  is the baryon density.  $\Im f_\omega(0)$  can be evaluated using the optical theorem from the total  $\omega N$  cross section  $\sigma_{\omega N}^{tot}$  as

$$\Im f_\omega(0) = \frac{p_\omega}{4\pi} \sigma_{\omega N}^{tot}, \quad (2)$$

with  $p_\omega$  denoting the  $\omega$ -meson momentum.

The partial  $\omega N \rightarrow \pi N$  cross section can be obtained from the  $\pi N \rightarrow \omega N$  data using detailed balance. The total  $\omega N$  cross section consists of several different final channels, but the  $\omega N \rightarrow \pi N$  channel is believed to be the one numerically most important. In any case, knowledge of this inelastic channel provides at least a lower bound for the imaginary part of the forward scattering amplitude  $\Im f_\omega(0)$ . The above procedure was extensively applied in the literature [11, 12].

3) The feasibility of producing nuclear bound states of  $\omega$ -mesons [18, 19] can be estimated reliably in terms of

the effective  $\omega N$  scattering length, which again is dominantly given by the  $\pi^- p \rightarrow \omega n$  data near the reaction threshold [13]. Thus the data given in Ref. [3] directly lead to an estimate of the possible existence of  $\omega$ -mesonic nuclei.

In addition, it should be stressed that the near-threshold production of the  $\omega$ -mesons in the  $pd \rightarrow \omega^3 He$  reaction [20] indicates that the squared matrix element  $|\mathcal{M}|^2$  strongly decreases starting from the center-of-mass  $\omega$ -meson momentum  $q_\omega \simeq 120$  MeV/c to the reaction threshold where  $q_\omega = 0$ . Within the indicated  $q_\omega$  range the reduction of  $|\mathcal{M}|^2$  accounts for a factor of almost 4. As we discussed above, exactly the same reduction within the same range of the  $\omega$ -meson momenta  $q_\omega \leq 120$  MeV/c was claimed for the  $\pi^- p \rightarrow \omega n$  measurements [3].

It should be stressed, however, that the squared matrix element  $|\mathcal{M}|^2$  evaluated from the data on other heavy mesons as  $\eta'$  [21] and  $\phi$  [22] production in  $\pi N$  reactions did not show such a strong near-threshold suppression. This difference might be ascribed to the fact that the  $\eta'$  and  $\phi$ -meson widths are significantly smaller than that of the  $\omega$ .

The above motivation still does not cover all subjects in which  $\pi^- p \rightarrow \omega n$  data were used. In a recent publication it was argued that the experiments as described, e.g., in Ref. [3] were misinterpreted [4]. The authors proposed a correction factor that completely removed the above-mentioned strong energy dependence from the cross section. If confirmed, this factor would answer why all microscopic calculations performed so far [23] failed to reproduce the energy dependence of the data correctly. The main conclusion of this work will be to argue, that, although the formalism derived in ref. [1] is correct, it was applied improperly in refs. [2, 3, 20]. Since our argument rests on circumstantial evidence only, we strongly call for a remeasurement of the reaction  $\pi N \rightarrow \omega N$  close to the threshold.

The paper is organized as follows. In Sec. II we summarize the current status of the  $\pi N \rightarrow \omega N$  data and provide the data interpretation as it was given in the Ref. [3]. In Sec. III we derive an analytical formula for the quantity measured in Refs. [1, 2, 3]. In Sec. IV we describe the Monte Carlo simulations of the  $\pi^- p \rightarrow \omega n$  measurements. The evaluation of the imaginary part of the  $\omega N$  scattering length from the  $\pi N \rightarrow \omega N$  data is given in Sec. V. The paper concludes with a summary.

## II. EXPERIMENTAL DATA

In this section we summarize the current status of the data available for the  $\pi N \rightarrow \omega N$  total reaction cross section at pion beam energies close to the nominal production threshold, which is given by the pole mass  $M_\omega = 781.94$  MeV of the  $\omega$ -meson. There are three publications from the same group that report results for  $\pi^- p \rightarrow \omega n$  measurements close to the nominal  $\omega$  production threshold [1, 2, 3]. The data of highest quality are

presented in the paper of Karami et al. [3], as shown in Table I. The experimental procedure can be sketched as follows.

The measurements were done at 33 different pion beam momenta  $p_\pi$  scanning the range from 1040 to 1265 MeV/c. The beam momentum resolution was  $\Delta p_\pi / p_\pi \simeq 0.8\%$ , so each pion momentum setting additionally covered a range  $\simeq 8$ -10 MeV. At each pion beam momentum the neutrons were collected in 60 counters set within the angular range from  $2.5^\circ$  to  $25.1^\circ$  from the beam direction.

The final statistics were regrouped in 2 MeV/c wide incident pion momentum bins with intensity about  $10^8$  pions per bin. At each beam momentum the final neutron momentum  $q_n$  and the neutron emission angle  $\theta^*$  in the center of mass system, as well as the flux, were determined. The incident flux at all momenta was well fixed by weighting each event proportionally to the total number of the incident pions at its particular momentum.

The data were distributed over 10 intervals of the neutron momenta  $q_n$  and 10 intervals of  $\cos\theta^*$ . This procedure is equivalent to an integration over incoming  $\pi$ -meson momenta for a fixed produced neutron momentum and angle.

For every bin in  $q_n$  and  $\cos\theta^*$  the missing mass spectrum  $d\sigma_{exp}/dm$  was reconstructed in order to separate the  $\omega$ -meson spectral distribution and the background [26]. The  $d\sigma_{exp}/dm$  spectra were then fitted by a sum of an  $\omega$ -meson spectral function and a low-order polynomial. The fitting allowed separation of the background and  $\omega$ -meson signal.

The spectral distribution  $d\sigma_{exp}/dm$  at fixed intervals of  $q_n$  and  $\cos\theta^*$  was obtained by scanning or integrating over the pion beam momentum  $p_\pi$ . To replace the integration over  $p_\pi$  by an integration of the reconstructed missing mass spectra  $d\sigma_{exp}/dm$  over the mass  $m$ , the data were corrected by a corresponding Jacobian  $\partial p_\pi / \partial m$ . The Jacobian weakly depends on the beam momentum. Neither in ref. [3] nor in ref. [2] the inclusion of an additional Jacobian is mentioned. We come back to this point below.

Finally the differential  $\pi^- p \rightarrow \omega n$  cross sections were determined for all  $10 \times 10$  intervals in neutron momentum  $q_n$  and  $\cos\theta^*$ . The differential  $d\sigma/d\Omega$  cross sections shown in Ref. [3] for the different intervals of the neutron momenta are almost isotropic. The cross sections indicated in Table I were obtained by summing over the differential  $d\sigma/d\Omega$  cross sections for each neutron momentum interval. The  $q_n$  intervals were specified for the central value of the cms neutron momenta  $P^*$  given within the bin  $\pm \Delta P/2$ .

The data collected in that way were interpreted as two-body  $\pi^- p \rightarrow \omega n$  reaction cross sections  $\sigma_{2b}$ . These cross sections have been considered as those for a stable  $\omega$ -meson production, since the beam momentum integration eliminates the dependence on the  $\omega$  width. The

TABLE I: The  $\pi^- p \rightarrow \omega n$  cross section  $\sigma$  measured by Karami et al. [3] for different intervals of the final neutron momenta  $P^* \pm \Delta P/2$  in the center of mass system. Also are shown the reduced cross sections given by the ratio  $\sigma/P^*$ .

$P^*$ (MeV/c)	$\Delta P$ (MeV/c)	$\sigma_{exp}$ ( $\mu b$ )	$\sigma_{exp}/P^*$ ( $\mu b/(\text{MeV}/c)$ )
50	20	197 $\pm$ 18	3.94 $\pm$ 0.36
70	20	339 $\pm$ 26	4.84 $\pm$ 0.37
90	20	577 $\pm$ 40	6.41 $\pm$ 0.44
110	20	830 $\pm$ 50	7.55 $\pm$ 0.45
130	20	1118 $\pm$ 71	8.60 $\pm$ 0.55
150	20	1350 $\pm$ 80	9.00 $\pm$ 0.53
170	20	1510 $\pm$ 74	8.88 $\pm$ 0.44
190	20	1560 $\pm$ 83	8.21 $\pm$ 0.44

two-body reaction cross section is given explicitly by [24]

$$\sigma_{2b} = 6 \frac{2}{3} \frac{1}{16\pi s} \frac{q_n}{q_\pi} |\mathcal{M}|^2, \quad (3)$$

where the factor of 6 accounts for the summation over the number of final spin states, the factor 2/3 is the isospin factor relating particle basis and isospin basis,  $\mathcal{M}$  is the spin averaged matrix element in the isospin basis and  $s$  stands for the squared invariant collision energy. Furthermore, in Eq. (3)  $q_\pi$  and  $q_n$  are the incident and final center of mass momenta, respectively, with

$$q_\pi = \frac{\lambda^{1/2}(s, m_\pi^2, m_N^2)}{2\sqrt{s}},$$

$$q_n = \frac{\lambda^{1/2}(s, M_\omega^2, m_n^2)}{2\sqrt{s}}, \quad (4)$$

where  $m_n$  and  $m_\pi$  are the nucleon and pion masses, respectively,  $M_\omega=781.94$  MeV is the pole mass of the  $\omega$ -meson and the function  $\lambda$  is given by

$$\lambda(x, y, z) = (x - y - z)^2 - 4yz. \quad (5)$$

In line with Eq. (3), in order to extract the energy dependence of the matrix element squared  $|\mathcal{M}|^2$  one has to divide the measured cross sections by the phase space volume of the two-body final state. Already in the original publication the results on the reduced cross section  $\sigma/P^*$  (the last column of the Table I) was given and the strong momentum dependence of the  $\pi^+ n \rightarrow \omega p$  reduced cross section was interpreted as a strong momentum dependence of the reaction matrix element.

The interpretation of the results given in Refs. [1, 2, 3] as a two-body reaction cross section was also used in the Landoldt-Börnstein compilation of elementary reactions cross sections [5] for both  $\pi^- p \rightarrow \omega n$  and  $\pi^+ n \rightarrow \omega p$  total cross sections. There the data are shown for fixed beam momentum corresponding to the center of mass momenta given in the experimental source. Note that the final center of mass momenta  $q_n$  given in the experimental paper (here reproduced in Table I) do not match the

initial pion beam momenta given in the compilation [5] (here reproduced in Table II) when calculated under the assumption, that a stable omega with its nominal mass is produced. How the values for  $p_\pi$  in Ref. [5] where determined is unclear to us.

TABLE II: The  $\pi^- p \rightarrow \omega n$  reaction cross section  $\sigma$  and its uncertainty  $\Delta\sigma$  as given in the Landolt-Börnstein compilation [5] at the laboratory pion beam momenta  $p_\pi$  range from 1097 to 1170 MeV/c. Also shown are the matrix element squared  $|\mathcal{M}|^2$  evaluated by Eq. (3) and the final neutron momentum  $q_n$  in the center of mass system given by Eq. (4).

$p_\pi$ (GeV/c)	cross section $\sigma$ ( $\mu b$ )	error $\Delta\sigma$ ( $\mu b$ )	$ \mathcal{M} ^2$	$q_n$ (MeV/c)
1.097	197	18	182 $\pm$ 17	62
1.102	339	26	250 $\pm$ 19	78
1.109	577	40	347 $\pm$ 24	97
1.118	830	50	420 $\pm$ 25	116
1.128	1118	71	495 $\pm$ 31	135
1.140	1350	80	531 $\pm$ 31	154
1.154	1510	74	535 $\pm$ 26	174
1.170	1560	83	504 $\pm$ 27	193

The spin averaged squared matrix element  $|\mathcal{M}|^2$  defined through Eq. (3) is shown in Fig.1 as well as in Table II as a function of the neutron momentum  $q_n$ . The results are shown for the  $\pi^- p \rightarrow \omega n$  (triangles) and  $\pi^+ n \rightarrow \omega p$  (squares) reactions. The data [5] on the  $\pi^- p \rightarrow \omega n$  reaction for laboratory pion beam momenta between 1.097 and 1.17 GeV/c are shown by the circles.

Fig.1 illustrates the very strong momentum dependence of the squared matrix element near the reaction threshold at  $q_n \leq 200$  MeV/c mentioned above. Within the short range of the neutron momentum  $q_n$  from 154 to 62 MeV/c  $|\mathcal{M}|^2$  decreases almost by a factor of 3.

Summarizing, there are three potential sources of energy dependence of the  $\pi^- p \rightarrow \omega n$  total cross section close to the nominal  $\omega$  production threshold: the phase space, the width of the  $\omega$ -meson and the  $\pi^- p \rightarrow \omega n$  transition amplitude. It is the last quantity  $|\mathcal{M}|^2$  that contains all the  $\omega$  production dynamics. In the energy regime of interest here the width effect on the energy dependence of the cross section is quite large. As was described above, to remove this effect from the data in a model-independent way, the authors of Ref.[1, 2, 3] proposed to integrate over some range of initial pion momenta  $p_\pi$  for a fixed final neutron momentum labeled  $P^*$ . It was shown in ref. [1] how the count rates can be related to the cross sections. Due to the aforementioned difficulties for model studies to account for the resulting energy dependence of the cross section we repeat here the derivation from Binnie et al. and check the approximations made along the line with an event-by-event simulation.

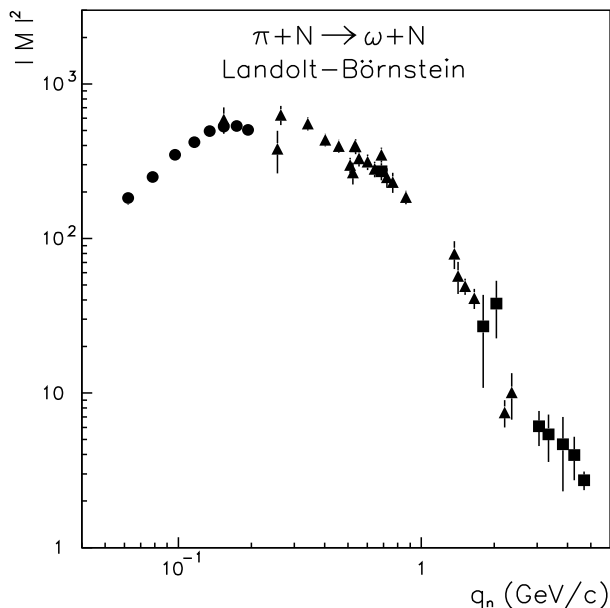


FIG. 1: The spin averaged matrix element squared  $|\mathcal{M}|^2$  evaluated by Eq. (3) from the total  $\pi^-p \rightarrow \omega n$  (triangles) and  $\pi^+n \rightarrow \omega p$  (squares) cross sections taken from the compilation [5] as a function of the final neutron momentum  $q_n$  in the center of mass system given by Eq. (4). The  $\pi^-p \rightarrow \omega n$  data quoted [5] for the laboratory pion beam momenta  $1.097 \leq p_\pi \leq 1.17$  GeV/c are shown by the circles.

### III. ENERGY DEPENDENCE OF THE CROSS SECTION

In Ref. [4] it was argued that the energy dependence of the  $\pi^-p \rightarrow \omega n$  reaction matrix element as shown in Fig. 1 can be traced to a misleading interpretation of the measured count rates. The basic findings were that it is indeed possible to extract the transition matrix element independent of the shape of the mass distribution of the resonance, however—in contradiction to the claims of Refs.[1, 2, 3]—it was argued that the energy dependence of the count rates is different from that of the two-body reaction. As a consequence it was claimed, that the above mentioned energy dependence of the matrix element squared  $|\mathcal{M}|^2$  is a purely kinematical effect. In this section we want to check this claim by repeating the derivation of Binnie et al.. As it will turn out, the theoretical part of Ref. [1] is correct, however, there is a chance of misinterpretation of the final formula (formula (10) in Ref. [1]) which might have lead to a misuse of the technique. We will come back to this point below. In addition, we regard the following discussion as usefull for future experiments for it is somewhat more compact than the original presentation of ref. [1].

Let us start with the cross section for  $\pi N \rightarrow XN$  reaction, where  $X$  denotes the decay products of the unstable meson. The reaction cross section can be expressed as

$$d\sigma = (2\pi)^4 \frac{4}{q_\pi \sqrt{s}} |\mathcal{M}|^2 d\zeta. \quad (6)$$

As in Eq. (3)  $q_\pi$  denotes the cms momentum of the initial pion and  $\mathcal{M}$  the spin averaged invariant matrix element. The factor of four is a combination of spin and isospin factors, as is given by Eq. (3). The trivial energy dependences of the reaction cross section are collected in the function  $\zeta$ , which is defined as

$$d\zeta = d\Phi_{k+1}(p; p_n, p_1, \dots, p_k) |D(m^2)W(p_1, \dots, p_k)|^2, \quad (7)$$

where we assume the unstable meson, whose propagation is described by  $D(m^2)$ , to decay into the  $k$  particles through the vertex function  $W$ . Here  $m^2$  is the total invariant mass of the  $k$  final decay particles with  $m^2 = (\sum p_i)^2$ , where the  $p_i$ ,  $i = 1..k$  denote the corresponding four-momenta. Furthermore, the total initial four-momentum is denoted by  $p$ . The phase space of the final  $k$  particles and the final nucleon with the four-momentum  $p_n$  is defined as

$$d\Phi_{k+1}(p; p_n, p_1, \dots, p_k) = \delta^4(p - p_n - \sum p_i) \times \frac{d^3 p_n}{(2\pi)^3} \frac{1}{2E_n} \prod_i \frac{d^3 p_i}{(2\pi)^3 2\omega_i}, \quad (8)$$

where  $E_n$  and  $\omega_i$  are the energy of the final nucleon and  $i$ -th decay particle, respectively.

Using the unitarity relation we can introduce the spectral function  $\rho$  as

$$(2\pi)^3 \int d\Phi_k(p_X; p_1, \dots, p_k) |D(m^2)W|^2 = -\frac{1}{\pi} \Im D(m^2) =: \rho(m^2). \quad (9)$$

A standard choice for the spectral function is that of a Breit-Wigner resonance,

$$\rho(m^2) = \frac{1}{\pi} \frac{M_\omega \Gamma_\omega}{(m^2 - M_\omega^2)^2 + M_\omega^2 \Gamma_\omega^2}, \quad (10)$$

where  $M_\omega$  and  $\Gamma_\omega$  are the pole mass and width of the  $\omega$ -meson, respectively. It is this form that we will use in the evaluation of intermediate results. For the final result, however, the exact shape of the spectral function is irrelevant. All that we will use is the normalization condition, namely

$$\int dm^2 \rho(m^2) = 1. \quad (11)$$

Now we can rewrite Eq. (7) in the center of mass system as

$$d\zeta = \frac{1}{4(2\pi)^6} \rho(m^2) dm^2 \frac{d^3 q_n}{\omega E_n} \delta(\sqrt{s} - \omega - E_n) = \frac{1}{2(2\pi)^6} \rho(s - 2\sqrt{s}E_n + m_n^2) \frac{d^3 q_n}{E_n}, \quad (12)$$

where  $\omega = \sqrt{m^2 + \vec{q}_n^2}$  is the energy of the final unstable meson state with the total invariant mass  $m$  and  $q_n$  denotes the momentum of the final nucleon in the center of mass system.

Finally, by introducing Eq. (12) into the Eq. (6), we obtain the differential cross section as a function of the nucleon momentum:

$$\frac{d\sigma}{dq_n} = \frac{1}{2\pi q_\pi \sqrt{s}} \frac{q_n^2}{E_n} |\mathcal{M}|^2 \rho(s - 2\sqrt{s}E_{q_n} + m_n^2). \quad (13)$$

This formula agrees with that used in Ref. [22] up to differences in the normalisation. Note that in the limit of vanishing width of the unstable particle Eq. (13) transforms into the two-body cross section of Eq. (3) for the production of particles with fixed masses, since

$$\lim_{\Gamma \rightarrow 0} \rho(s - 2\sqrt{s}E_n + m_n^2) = \frac{E'_n}{2\sqrt{s}} \left( \frac{1}{q'_n} \right) \delta(q_n - q'_n), \quad (14)$$

where  $E'_n$  and  $q'_n$  denote the energy and relative momentum of the produced stable particles. It is interesting to investigate for what values of  $\Gamma$  the right hand side of Eq. (14) is a good approximation to the left hand side. Naturally, the parameter that controls the behavior of the cross section should depend on the energy and the width of the decaying particle as well as the resolution of the detector. For the cross section to appear as a two-body cross section we should not resolve the decay particles any further. In Ref. [4] it was shown that for

$$\frac{2P^* \Delta P}{\mu \Gamma} \gg 1, \quad (15)$$

where  $\mu$  denotes the reduced mass of the  $\omega n$  system, the reaction rate behaves indeed like a two-body cross section. It should be obvious that the ratio  $\Delta P/\Gamma$  appears here, for this ratio measures how closely we look at the production rates. For a given detector resolution  $\Delta P$  we thus deduce a critical value for  $P^*$  below which deviations from the two-body behaviour should be expected on purely kinematical grounds. Using  $\Delta P = 20$  MeV as given in Table I we find that, for values of  $P^* \gg 90$  MeV, the cross section for a fixed energy should behave like a two-body cross section.

The solid lines in the Fig. 2 show the differential cross section  $d\sigma/dq_n$  calculated for the  $\pi^- p \rightarrow \omega n$  reaction at fixed  $\pi$ -meson momenta  $p_\pi$ . Here we employed the relativistic Breit-Wigner form as given in Eq. (10) for the  $\omega$ -meson spectral function. Furthermore, in this calculation, we employed the almost constant matrix element squared  $|\mathcal{M}|^2$ , as defined in Eq. (34). The neutron spectra are shown in Fig. 2 for the  $q_n$  range studied by Karami et al. [3]. Fig. 2 shows that the differential cross section  $d\sigma/dq_n$  reflects the behavior of the spectral function.

Fig. 2 illustrates an important feature: namely, the differential cross section at different pion momenta, but at the same fixed neutron momentum are substantially different in absolute value. Naively one would expect that the  $d\sigma/dq_n$  are identical for different  $p_\pi$  but the same  $q_n$ . Note that the difference in the flux factor due to the different pion momenta is almost negligible within the range  $1 \leq p_\pi \leq 1.2$  GeV/c. The calculations by Eq. (4) clearly show an absolutely different situation, since the

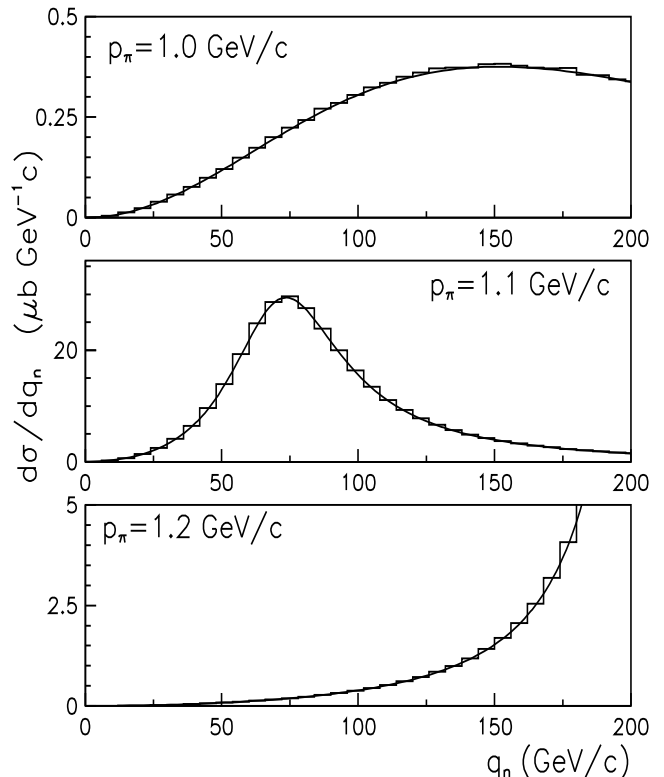


FIG. 2: The neutron momentum spectra calculated at different fixed pion beam momenta  $p_\pi$ . The histograms show the results from the event-by-event simulations, while the solid lines indicate the Eq. (4). The spectra are shown only for the neutron momenta  $q_n$  range covered by Karami experiment [3].

phase space dependence of the cross section can not be factored from the spectral function density.

It was the idea of Refs.[1, 2, 3] to remove the dependence on the spectral function from Eq. (13) through an integration over the initial pion momentum  $p_\pi$ . The necessary assumption is that the flux as well as the matrix element squared  $|\mathcal{M}|^2$  only weakly depend on the total collision energy when evaluated within a limited range of final  $q_n$  momenta. In addition, we need to assume that neither of the two vary significantly when  $m$  is varied within the range where the spectral function is large.

By integrating Eq. (2) over the laboratory  $\pi$ -meson momentum  $p_\pi$  we obtain the  $\pi^- p \rightarrow \omega n$  cross section for the range of the neutron cms momentum  $P^* \pm \Delta P/2$  as

$$\bar{\sigma}(P^*, \Delta P) = \int_{p_\pi^-}^{p_\pi^+} dp_\pi \frac{1}{\Delta P} \int_{q_-}^{q_+} dq_n \frac{d\sigma}{dq_n}, \quad (16)$$

where the limits of the integration over the neutron momentum are fixed by

$$q_\pm = P^* \pm \Delta P/2, \quad (17)$$

while the integration over the pion laboratory momentum were performed [3] within the range from 1040 to 1265 MeV/c.

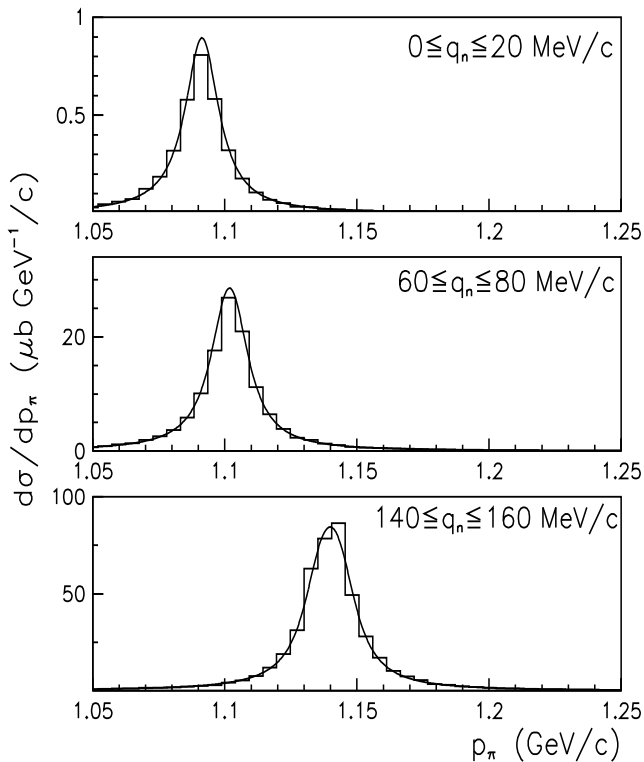


FIG. 3: The differential cross section as a function of the pion beam momentum  $p_\pi$  calculated for different ranges of neutron momenta  $q_n$ . The histograms are results from the event-by-event generator while the solid lines show the calculations using Eq. (16).

The solid lines in Fig. 3 show the neutron differential cross section as a function of the  $\pi$ -meson beam momentum calculated for the two different intervals of the neutron momenta. The shapes of the  $d\sigma/dp_\pi$  distributions reflects the Breit–Wigner spectral function distribution. The width is dominantly given by the  $\omega$ -width with a tiny correction from the spread in the outgoing momentum.

To remove the dependence on the spectral function  $\rho$ , we replace in Eq. (16) the integration over  $p_\pi$  by an integration over the invariant mass squared  $m^2$  and additionally impose the normalization condition of Eq. (11). As illustrated in Fig. 3 the  $p_\pi$  integration can be assumed to be done over an infinite range. Therefore, the  $\pi^-p \rightarrow \omega n$  cross section is given as

$$\bar{\sigma}(P^*, \Delta P) = \kappa \left[ P^{*2} + \frac{1}{12}(\Delta P)^2 \right] |\mathcal{M}|^2, \quad (18)$$

with

$$\kappa = \frac{1}{2\pi E_n q_\pi \sqrt{s}} \left( \frac{\partial p_\pi}{\partial m^2} \right), \quad (19)$$

where  $E_n = \sqrt{P^{*2} + m_n^2}$  and  $s$  denotes the invariant collision energy evaluated for the production of a stable  $\omega$ -meson with center of mass momentum  $P^*$ . The weakly

energy dependent Jacobian is given by

$$\left( \frac{\partial p_\pi}{\partial m^2} \right) \simeq \frac{s - m_\pi^2 - m_n^2}{4M_\omega m_n q_\pi}, \quad (20)$$

where we have used the non relativistic expression for the total energy of the  $\omega$ -meson.

The expression given in formula (18) agrees to eq. (10) of ref. [1] for an ideal detector and beam, which states, translated into the quantities used above

$$\bar{\sigma} = 2M_\omega \left( \frac{\partial p_\pi}{\partial m^2} \right) \frac{1}{\Delta P} \int_{\Delta\tau} d\tau dx^L J_\tau \frac{d\sigma}{dt}, \quad (21)$$

where  $x^L$  denotes the cosine of the scattering angle in the lab frame,  $\tau$  denotes the time of flight of the outgoing neutron and  $J_\tau$  is the Jacobian relating the system  $(\cos(\theta), \tau)$  to  $(m, t)$  (c.f. eq. (6) in ref. [1])

$$J_\tau = \frac{2(q_n^L)^4 p_\pi m_N}{(E_n^L)^2 M_\omega d}, \quad (22)$$

where  $d$  denotes the flight distance for the neutrons and  $q_n^L(E_n^L)$  denote the neutron momentum (energy) in the laboratory frame. In addition, for an isotropic matrix-element

$$\begin{aligned} \frac{d\sigma}{dt} &= \left( \frac{\pi E_n}{2q_n q_n^2 \sqrt{s}} \right) \int dm^2 \frac{d^3\sigma}{dq_n d\Omega} \\ &= \frac{1}{16\pi q_\pi^2 s} |\mathcal{M}|^2. \end{aligned} \quad (23)$$

Thus, at this stage it seems as if the experiments of refs. [1, 2, 3, 20] where analysed properly. However, from what is written in refs. [2, 3] it is unclear, if  $\sigma_{exp}$ , defined through

$$\bar{\sigma}(P^*, \Delta P) = 2M_\omega \left( \frac{\partial p_\pi}{\partial m^2} \right) \sigma_{exp}(P^*). \quad (24)$$

is given, or  $d\sigma/dt$  as it can be extracted using eq. (21). The former option corresponds to interpreting  $J_\tau$  in eq. (21) as  $J_{(\tau, q_n)}$ —the Jacobian that connects  $(\cos(\theta), \tau)$  to  $(q_n, t)$ , where

$$J_{(\tau, q_n)} = \frac{\tilde{\mu}}{q_n} J_\tau, \quad (25)$$

where  $\tilde{\mu} = M_\omega E_n / \sqrt{s}$ , which reduces to the reduced mass of the final state in the non-relativistic limit. This interpretation of the Jacobian appearing in eq. (21) is natural (though wrong) to the extend that the cut in the outgoing neutron momentum is given in terms of  $q_n$ , whereas eq. (21) is formulated in terms of the time of flight  $\tau$ . The following evidence supports, that this misinterpretation actually took place, namely

- both publications [2, 3] only mention that there is a Jacobian to be included without further comment whether they used  $J_\tau$  (given in eq. (22)) or  $J_{(\tau, q_n)}$  (given in eq. (25)), thus suggesting that only the naive one that connects the coordinate systems—namely  $J_{(\tau, q_n)}$  is used and

- in ref. [20] there is explicitly only the analog of  $J_{(\tau, q_n)}$  mentioned and no other. Note, the momentum dependence of the amplitude given in ref. [20] is consistent with that by Karami et al. [27].

Thus one may consider two options: *Either*  $J_\tau$  (c.f. eq. (22)) was indeed included in the experimental analysis of Refs. [1, 2, 3, 20] and the data. Then the strong energy dependence as shown in Fig. 1 is physical.

Or the experimental data were analysed using  $J_{(\tau, q_n)}$  as given by eq. (25).

In what follows we investigate the consequences of the second option. In other words, we study the implications of the *assumption* that it was  $\sigma_{exp}$  defined in eq. (24) that was given in the experimental papers [2, 3].

Matching Eqs. (24) and (18), we arrive at the central formula of this manuscript, providing the relation between the measured cross section [1, 2, 3] and the squared matrix element  $|\mathcal{M}|^2$  of the  $\pi^- p \rightarrow \omega n$  reaction, namely

$$\sigma_{exp} = \frac{1}{4\pi q_\pi s \tilde{\mu}} (P^{*2} + (\Delta P)^2/12) |\mathcal{M}|^2. \quad (26)$$

One might wonder why the resolution of the neutron detector enters the final expression. On a second thought this should be quite obvious, since for every given value of  $\Delta P$  there will be a count rate even for a minimal value of  $P^*$ . This is most clearly demonstrated in the uppermost panel of Fig. (3).

By construction,  $\mathcal{M}$  is the matrix element for the reaction  $\pi^- p \rightarrow \omega n$  considering the  $\omega$ -meson as a stable particle, since the width of the omega was treated explicitly. We can therefore define an effective two-body cross section  $\sigma^{eff}$  given by Eq. (3) in terms of the cross section  $\sigma_{exp}$  measured in Ref. [3]:

$$\sigma^{eff} = \frac{\tilde{\mu} P^*}{P^{*2} + (\Delta P)^2/12} \sigma_{exp}, \quad (27)$$

Therefore, the effective cross section  $\sigma^{eff}$  is the  $\pi^- p \rightarrow \omega n$  total reaction cross section taken under the assumption that the produced  $\omega$ -meson is stable with the fixed mass  $M_\omega = 781.94$  MeV. In Table III we provide the corrected cross section  $\sigma^{eff}$  based on the hypothesis that the formalism given in Ref. [1] was applied improperly. The corrected  $\pi^- p \rightarrow \omega n$  reaction cross sections deviate from the results quoted in the compilation [5] by a factor up to 8 within the range of pion beam momenta  $1094 \leq p_\pi \leq 1167$  MeV/c.

We can now evaluate the corrected matrix element squared  $|\mathcal{M}|^2$  from the  $\pi^- p \rightarrow \omega n$  data employing Eq. (26). The results are shown in Fig. 4 and clearly illustrate that the corrected matrix element is in line with the other data and does not indicate any pathological energy dependence at small neutron momenta. The resulting energy dependence is in a lot better agreement with that of model studies [23]. This could be taken as further evidence, that indeed the formalism derived in Ref. [1] was applied improperly.

TABLE III: The corrected effective  $\pi^- p \rightarrow \omega n$  cross section  $\sigma^{eff}$  as derived by us. The second to last column contains the error as it is derived directly from the data [3], whereas in the error given in the last column the uncertainty of the neutron momentum  $P^*$  is included as well. The relation between the central neutron momentum  $P^*$  and the pion beam momentum  $p_\pi$  is given by Eq. (4).

$P^*$ (MeV/c)	$p_\pi$ (MeV/c)	$\sigma^{eff}$ ( $\mu b$ )	$\delta\sigma_{exp}^{eff}$ ( $\mu b$ )	$\delta\sigma_{exp+P^*}^{eff}$ ( $\mu b$ )
50	1094	1656	151	364
70	1099	2049	157	332
90	1106	2720	189	356
110	1115	3206	193	350
130	1125	3656	232	365
150	1137	3828	227	341
170	1151	3780	185	289
190	1167	3494	186	262

#### IV. EVENT-BY-EVENT SIMULATIONS

In addition, to check the analytical calculations of the previous section, we also developed an event-by-event generator to simulate the experimental measurements described in Refs. [1, 2, 3]. In addition, this simulation allows us to discuss several aspects of the technique developed in Ref. [1] in detail.

In accordance with Ref. [3], the  $\pi^- p \rightarrow \omega n$  events were simulated at pion momenta randomly selected within the range between 1040 and 1265 MeV/c. At fixed pion momentum  $p_\pi$  the events were generated by the following method.

1. The flux factor was determined as

$$\mathcal{L} = 8\pi^2 \lambda^{1/2}(s, m_\pi^2, m_p^2), \quad (28)$$

where  $m_\pi$ ,  $m_p$  and  $m_n$  are the pion, proton and neutron masses, respectively and  $s$  is the squared invariant energy of the event given by

$$s = m_n^2 + m_\pi^2 + 2m_n \sqrt{p_\pi^2 + m_n^2}. \quad (29)$$

2. The squared  $\omega$ -meson mass  $m^2$  was randomly generated by the Breit-Wigner probability distribution as defined in Eq. (10).

3. The neutron momentum was calculated as

$$q_n = \frac{\lambda^{1/2}(s, m^2, m_n^2)}{2\sqrt{s}}, \quad (30)$$

and the phase space factor of the event is given as

$$\Phi = \pi \frac{\lambda^{1/2}(s, m^2, m_n^2)}{2s}. \quad (31)$$

4. Now each event at fixed pion beam momentum  $p_\pi$  and with certain  $\omega$ -meson mass  $m$  was accounted for with the weight [24]

$$W_{ev} = \frac{\Phi}{\mathcal{L}} 4|\mathcal{M}|^2. \quad (32)$$

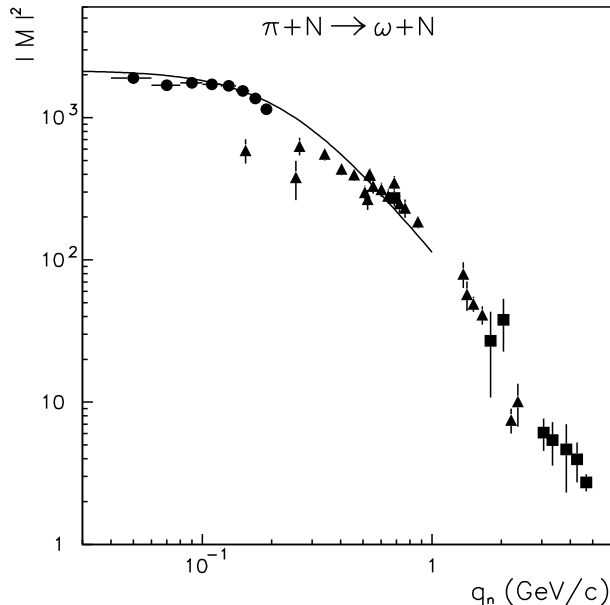


FIG. 4: The spin averaged matrix element squared  $|\mathcal{M}|^2$  extracted from the total  $\pi^-p \rightarrow \omega n$  (triangles) and  $\pi^+n \rightarrow \omega p$  (squares) cross sections taken from the compilation [5] as a function of the final neutron momentum  $q_n$ . The circles show the corrected matrix element squared evaluated using Eq. (26) for the data [3] on the  $\pi^-p \rightarrow \omega n$  reaction. The solid line shows the parametrization of the matrix element given by Eq. (34) with the parameters fixed by a fit of the event-by-event simulation of the data of Ref. [3].

As in Eq. (3),  $\mathcal{M}$  denotes the spin averaged matrix element in isospin basis and the factor of 4 stems from a combination of the number of final spin states and the isospin factor. Note that this expression agrees with that for a two-body cross section (c.f. Eq. (3)), however, in our analysis we treat the energy and mass dependence of  $q_n$  properly.

5. In order to ensure energy conservation we impose the kinematical condition  $W_{ev}=0$  when  $\sqrt{s} \leq m + m_n$ .

Now, to calculate the  $\pi^-p \rightarrow \omega n$  cross section at fixed pion momentum  $\sigma(p_\pi)$ , we generate  $N$  events and sum them as

$$\sigma(p_\pi) = \frac{1}{N} \sum_{ev=1}^{ev=N} W_{ev}. \quad (33)$$

As described in the previous section, in Ref. [3] the data are given not at fixed pion beam momenta, but at different ranges of the neutron momenta. At fixed pion beam momentum the reaction  $\pi^-p \rightarrow \omega n$  produces the neutron momentum spectrum rather than a fixed neutron momentum because of the variation of the  $\omega$ -meson mass. It can be well understood within the event-by-event simulations when proceeding from step 2 to step 3, as illustrated in Fig. 2. The histograms in Fig. 2 show the results from the Monte Carlo simulations, which are

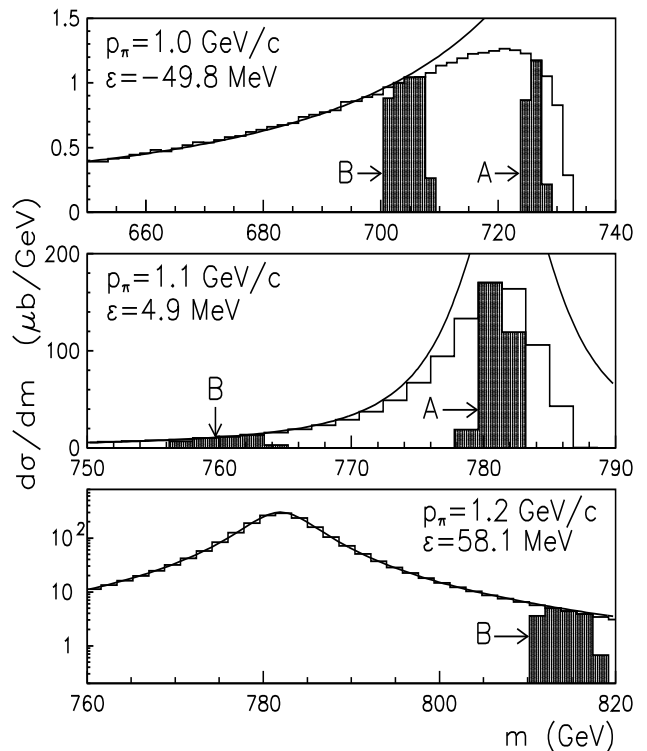


FIG. 5: The missing mass spectra calculated for the fixed pion momenta  $p_\pi$ . The full histograms show the results from the event-by-event generator. The solid lines indicate the Breit-Wigner distribution for the  $\omega$ -meson. The hatched histograms show the mass spectra for the neutron momenta ranges  $60 \leq q_n \leq 80$  MeV/c (A) and  $140 \leq q_n \leq 160$  MeV/c (B). The excess energy  $\epsilon = \sqrt{s} - m_n - M_\omega$ .

in agreement with the analytical evaluations.

Fig. 5 also shows the missing mass distribution simulated for the  $\pi^-p \rightarrow \omega n$  reaction at different fixed pion momenta. The histograms in Fig. 5 indicate the total missing mass spectra, while the solid lines indicate the relativistic Breit-Wigner distribution for the  $\omega$ -meson. It is clear that at low pion momenta only  $\omega$ -mesons with small masses can be produced because of the energy conservation imposed by the condition of step 5.

The hatched histograms in Fig. 5, moreover, show the missing mass spectra for the two neutron momenta ranges  $60 \leq q_n \leq 80$  MeV/c (A) and  $140 \leq q_n \leq 160$  MeV/c (B). Therefore, for a fixed range of final neutron momenta, the contribution from the different  $\omega$ -meson masses comes due to the different incident pion momenta. Fig. 5 most clearly illustrates the basic idea of the measurements [1, 2, 3]: namely to saturate the  $\omega$ -meson spectral function by scanning the pion beam momentum. As indicated by the hatched histograms, the  $\omega$  production cross sections at different  $\pi$ -meson momenta but at the same neutron momentum  $q_n$  substantially differ in absolute value.

An additional generation over the initial pion momentum  $p_\pi$  is required, randomly scanning the experimental



pion momentum range. After introducing the Jacobian defined in Eq. (20), we fit the experimental data [3] in order to extract the matrix element squared  $|\mathcal{M}|^2$  as well as its energy dependence. For the squared matrix element  $|\mathcal{M}|^2$  we assume an energy dependence given by

$$|\mathcal{M}|^2 = \frac{M_0^2}{1 + bq_n^2}, \quad (34)$$

with parameters  $M_0$  and  $b$  to be fit to the data of Ref. [3].

Fig. 6 shows the experimental results from Ref. [3] together with the results of the fit with the parameters

$$M_0^2 = (2.1 \pm 0.1) \times 10^3 \text{ and } b = (0.7 \pm 0.1) \text{ fm}^2. \quad (35)$$

The experimental cross sections  $\sigma_{exp}$  [3] are shown by the solid circles, while the boxes are our calculations. The size of the boxes shows the uncertainty in the extraction of the matrix element squared  $|\mathcal{M}|^2$  as well as the range of integration used for the neutron momentum as given by  $\Delta P$ .

Finally, the squared matrix element parametrized by Eqs. (34) and (35) fitted by using the Monte Carlo simulations to the experimental data [3] is shown by the solid line in the Fig. 4. It agrees well with the results derived analytically. We also find that the parametrization given by Eq. (34) works rather well over a wide energy range. Note that the fit was carried out on the basis the dataset of Ref. [3] only, thus only the momentum range from 50 to 200 MeV was fit.

## V. EVALUATION OF THE SCATTERING LENGTH

The matrix element at vanishing neutron momentum is a quantity of particular interest. In order to evaluate  $|\mathcal{M}|^2$  at  $q_n=0$  we fit the results of the Fig. 7 with a polynomial in  $q_n^2$  as suggested in Ref. [11]

$$|\mathcal{M}|^2 = a + bq_n^2 + cq_n^4. \quad (36)$$

We find for the corrected matrix element  $a = 2.0 \times 10^3$ ,  $b = -0.6 \text{ fm}^2$  and  $c = -0.3 \text{ fm}^4$  and therefore

$$\lim_{q_n \rightarrow 0} |\mathcal{M}|^2 = (2.0 \pm 0.4) \times 10^3. \quad (37)$$

It is reassuring that the different parametrization of Eq. (34) lead to the same value of the matrix element at threshold within the experimental accuracy.

It is now straight forward to extract a lower limit for the imaginary part of the elastic scattering length. Assuming that the  $\omega N \rightarrow \pi N$  reaction channel provides the most significant part of the inelasticity for the  $\omega N$  scattering, the value derived should be a reasonable estimate of the true imaginary part of the scattering length. Note that model calculations [13, 14] show that the  $\pi N$  channel indeed dominates the  $\omega N$  interaction.

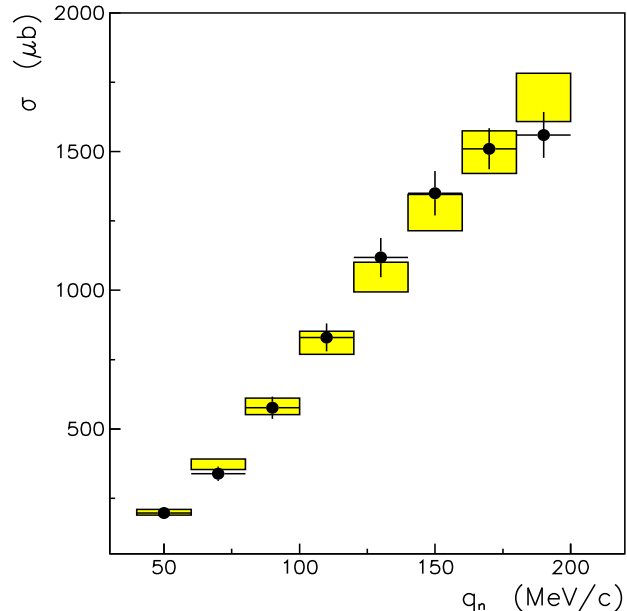


FIG. 6: The cross sections  $\sigma_{exp}$  measured at Karami experiment [3] at different intervals of a neutron momenta  $q_n$ . The experimental results [3] are shown by solid circles, while the boxes indicate our calculations. The size of the boxes illustrates the uncertainties in evaluation of the reaction matrix element  $|\mathcal{M}|$  and the neutron momentum interval.

We start with the  $S$ -matrix describing meson-baryon scattering near the  $\omega$ -meson production threshold and assume  $n$  physical final state channels to be relevant at this energy. The presentation is given in the isospin basis. Let the  $\omega N$  elastic channel be first, while the  $\pi N$  is second. The matrix element corresponding to the elastic  $\omega N$  channel is parametrized as

$$S_{11} := \eta \exp(2i\delta), \quad (38)$$

with  $\eta$  being the inelasticity in the  $\omega N$  scattering and  $\delta$  is the elastic scattering phase shift.

The unitarity constraint  $SS^\dagger = 1$  now translates into the relation

$$1 - \eta^2 = \sum_{i=2}^n (2s_i + 1) |S_{1i}|^2, \quad (39)$$

where the factor  $(2s_i + 1)$  contains the spin multiplicity of the particular channel  $i$ . Since all the contributions in the sum are positive, Eq. (39) directly leads to

$$1 - \eta^2 \geq 2|S_{12}|^2. \quad (40)$$

For s-wave scattering the relation between the  $S$ -matrix and  $\mathcal{M}$  evaluated previously is given by

$$S_{ij} = \delta_{ij} - \frac{i}{2(2\pi)^3} \sqrt{\frac{\lambda_i \lambda_j}{\omega_i E_i \omega_j E_j}} (4\pi) \mathcal{M}_{ij}, \quad (41)$$

where

$$\lambda_i = \pi \frac{E_i \omega_i}{\sqrt{s}} p_i, \quad (42)$$

with  $p_i$  being the on-shell momentum in the cms of the particular system and  $E_i$  and  $\omega_i$  denoting the baryon and meson energy in that channel, respectively. Combining the two last equations leads to

$$1 - \eta^2 \geq \frac{2}{(4\pi)^2} q_n \frac{q_\pi}{s} |\mathcal{M}|^2, \quad (43)$$

where  $q_\pi$  and  $q_n$  are the incident pion and final nucleon momenta in the center of mass system, respectively.

The scattering amplitude  $f_{\omega N}$  in the  $\omega N$  channel is given by

$$f_{\omega N} = \frac{1}{2q_n i} (1 - \eta e^{2i\delta}), \quad (44)$$

and thus its imaginary part reads

$$\Im f_{\omega N} = -\frac{1}{2q_n} (1 - \eta \cos(2\delta)). \quad (45)$$

The low momentum behavior of both the inelasticity  $(1 - \eta)$  as well as the phase shift  $\delta$  is linear in the momentum. Therefore, close to the nominal  $\omega$  production threshold we evaluate the imaginary part of the  $\omega N$  scattering length  $\Im a_{\omega N}$  as

$$\Im a_{\omega N} := -\lim_{(q_n \rightarrow 0)} \Im f_{\omega N} \geq \frac{1}{2(4\pi)^2} \frac{q_\pi}{s} |\mathcal{M}|^2. \quad (46)$$

Note that this formula agrees with the one given in Ref. [11].

Finally we deduce for the imaginary part of the spin averaged scattering length

$$\Im a_{\omega N} \geq (0.24 \pm 0.05) \text{ fm}. \quad (47)$$

As can be seen from Fig. 7, the value for the corrected squared matrix element at threshold changed by more than an order of magnitude. Since the lower limit for  $\Im a_{\omega N}$  scales linearly with the squared matrix element, our bound naturally is significantly stronger than those present in the current literature. For instance, in Ref. [11] a value  $\Im a_{\omega N} \geq 0.02$  fm is given (Note: in Ref. [11] the scattering length was deduced including the  $\pi^- p$  channel only. To include the  $\pi^0 n$  isotopic channel the result of Ref. [11] was multiplied with the isospin factor 3/2 to allow comparison to our value).

## VI. SUMMARY

Using a Monte Carlo simulation as well as an analytical calculation we reinvestigated the experimental data of Refs. [1, 2, 3] Based on circumstantial evidence, we argued, that the formalism derived correctly in Ref. [1] was

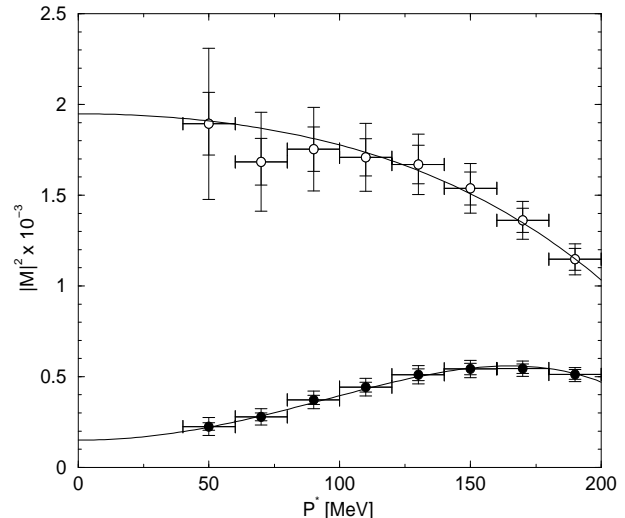


FIG. 7: The matrix element extracted from the data of Ref. [3]. The opaque circles denote the corrected matrix element using Eq. (27) whereas the filled circles show the uncorrected result. The small error bars are those from the data only, whereas the large error bars include the uncertainty in  $P^*$ , given by  $\Delta P=20$  MeV. The solid lines are polynomial fits to the data.

improperly applied in the analyses. A purely kinematical factor not only corrects this error and removes the unusual energy dependence resulting from the primary analysis, but also keeps the data in accordance with the world data set.

Based on the modified data we extracted a value for a lower bound the imaginary part of the elastic  $\omega N$  scattering length. The new value is larger by an order of magnitude compared than that used in the literature so far [11]. As should be clear from the discussion in the introduction, a large change in the imaginary part of the scattering length should have a large effect on estimates for both the in medium width of the omega as well as the existence of  $\omega$ -nucleus bound states.

We would like to stress that we call for a remeasurement of the  $\pi N \rightarrow \omega N$  reaction in the kinematics close to the nominal  $\omega$  threshold given the importance of this reaction, as outlined in the introduction. This remeasurement will not only allow to confirm the claims of this work but should also fill the gap in the experimental data between 200 and 500 MeV/c final center of mass momenta.

## VII. ACKNOWLEDGMENT

We appreciate usefull discussions with J. Durso, A. Kudrnyastev, U. Mosel, K. Nakayama, G. Penner and C. Wilkin. We also would wish to thank J. Durso for careful reading of the manuscript.

## REFERENCES

- [1] D.M. Binnie et al. Phys. Rev. D **8**, 2789 (1973).
- [2] J. Keyne et al., Phys. Rev. D **14**, 28 (1976).
- [3] H. Karami et al., Nucl. Phys. B **154**, 503 (1979).
- [4] C. Hanhart and A. Kudryavtsev, Eur. Phys. J. A **6**, 325 (1999).
- [5] Landoldt–Börnstein, New Series **I/12a**.
- [6] N. Isgur and G. Karl, Phys. Lett. B **72**, 109 (1977); R. Koniuk and N. Isgur, Phys. Rev. D **21**, 1868 (1980); N. Isgur and G. Karl, Phys. Rev. D **23**, 817 (1981).
- [7] S. Capstick and W. Roberts, Phys. Rev. D **49**, 4570 (1994); Q. Zhao, H. Li and C. Bennhold, Phys. Rev. C **58**, 2393 (1998); Q. Zhao, H. Li and C. Bennhold, Phys. Lett. B **436**, 42 (1998).
- [8] C. Wilkin, talk at 8th International Conference on the Structure of Baryons (Baryons 98), published in the proceedings and nucl-th/9810047
- [9] T. Feuster and U. Mosel, Phys. Rev. C **58**, 458 (1998).
- [10] T. Feuster and U. Mosel, Phys. Rev. C **59**, 460 (1999).
- [11] B. Friman, Acta Phys. Polon. B **29**, 3195 (1998).
- [12] M. Lutz, B. Friman and G. Wolf, Nucl. Phys. A **661**, 526 (1999).
- [13] F. Klingl, T. Waas and W. Weise, Nucl. Phys. A **650**, 299 (1999).
- [14] G.I. Lykasov et al., Eur. Phys. J. A **6**, 71 (1999).
- [15] W. Lenz, Z. Phys. **56**, 778 (1929).
- [16] C.D. Dover, J. Hüfner and R.H. Lemmer, Ann Phys. **66**, 248 (1971).
- [17] M. Lutz, A. Steiner and W. Weise, Nucl. Phys. A **574**, 755 (1994).
- [18] K. Tsushima, D.H. Lu, A.W. Thomas and K. Saito, Phys. Lett. B **443**, 26 (1998).
- [19] T. Yamazaki et al., Z. Phys. A **355**, 219 (1996); R.S. Hayano, Nucl. Phys. A **680**, 125 (2000); R.S. Hayano, S. Hirenzaki and A. Gillitzer, Eur. Phys. J. A **6**, 99 (1999); E. Marco and W. Weise, Phys. Lett. B **502**, 59 (2001).
- [20] R. Wurzinger et al., Phys. Rev. C **51**, R443 (1995).
- [21] A. Sibirtsev and W. Cassing, Eur. Phys. J. A **2**, 333 (1998).
- [22] A. Sibirtsev and W. Cassing, Eur. Phys. J. A **7**, 407 (1998).
- [23] M. Lutz, B. Friman and G. Wolf, Nucl. Phys. A **661** (1999) 526; F. Klingl, Ph.D. thesis, TU Munich, 1998; G. Penner and U. Mosel, nucl-th/0103060.
- [24] E. Byckling and K. Kajantie, Particle Kinematics, John Wiley and Sons (1973).
- [25] Actually, in the first version of this paper we also fell into this trap. We acknowledge the discussions with G. Penner that helped us to understand the work of Ref. [1].
- [26] Here we introduce the label *exp* to make explicit that this is the quantity measured. We will talk about its interpretation in the next section.
- [27] Yu.N. Uzikov, private communication.